www.MaterialsViews.com

Metal–Carbon Hybrid Electrocatalysts Derived from Ion-Exchange Resin Containing Heavy Metals for Efficient Hydrogen Evolution Reaction

Yucheng Zhou, Weijia Zhou, Dongman Hou, Guoqiang Li, Jinquan Wan, Chunhua Feng, Zhenghua Tang, and Shaowei Chen**

***T**ransition metal–carbon hybrids have been proposed as efficient electrocatalysts for hydrogen evolution reaction (HER) in acidic media. Herein, effective HER electrocatalysts based on metal–carbon composites are prepared by controlled pyrolysis of resin containing a variety of heavy metals. For the first time, Cr_2O_3 nanoparticles of 3–6 nm in diameter homogeneously dispersed in the resulting porous carbon framework (Cr–C hybrid) is synthesized as efficient HER electrocatalyst. Electrochemical measurements show that Cr–C hybrids display a high HER activity with an onset potential of –49 mV (vs reversible hydrogen electrode), a Tafel slope of 90 mV dec^{-1}, a large catalytic current density of 10 mA cm^{-2} at –123 mV, and the prominent electrochemical durability. X-ray photoelectron spectroscopic measurements confirm that electron transfer occurs from Cr_2O_3 into carbon, which is consistent with the reported metal@carbon systems. The obtained correlation between metals and HER activities may be exploited as a rational guideline in the design and engineering of HER electrocatalysts.*

Y. C. Zhou, Prof. W. J. Zhou, Prof. J. Q. Wan, Prof. C. H. Feng, Prof. Z. H. Tang, Prof. S. W. Chen
New Energy Research Institute
School of Environment and Energy
South China University of Technology
Guangzhou Higher Education Mega Center
Guangzhou 510006, P. R. China
E-mail: eszhouwj@scut.edu.cn; Shaowei@ucsc.edu

D. M. Hou, Prof. G. Q. Li
State Key Laboratory of Luminescent Materials and Devices
South China University of Technology
381 Wushan Road, Guangzhou 510641, P. R. China

Prof. J. Q. Wan, Prof. C. H. Feng
The Key Lab of Pollution Control and Ecosystem Restoration in Industry Clusters
Ministry of Education
South China University of Technology
Guangzhou Higher Education Mega Centre
Guangzhou 510006, P. R. China

Prof. S. W. Chen
Department of Chemistry and Biochemistry
University of California
1156 High Street, Santa Cruz, CA 95064, USA

DOI: 10.1002/smll.201503100

1. Introduction

Hydrogen, the cleanest fuel, has long been expected to play an important role in our future energy needs.[1] Electrochemical water splitting is an effective and environmentally friendly method to produce hydrogen.[2–6] One of the key challenges, however, is the development of efficient and stable catalysts based on inexpensive and earth-abundant elements.[7–12] For instance, nonprecious transition metals (e.g., Co and Ni) have been engineered as the active elements for hydrogen evolution reaction (HER) electrocatalysis.[12,13] Recently, Bao and co-workers reported that CoNi metal particles wrapped in ultrathin graphene layers significantly enhanced electron penetration,[14–17] and the active sites were ascribed to the carbon atoms whose density of electronic states was modulated by the transition metal elements. In another study, Tavakkoli et al. observed similar behaviors by employing single-shell carbon-encapsulated Fe nanoparticles for HER.[18] However, up until now, the core metals have been restricted to only a small number of transition metals, such as Fe, Co, and Ni. Hence, is it possible to extend the study to other metals? More importantly, will

these metals also promote the HER catalytic activity of the carbon shell?

With the rapid industrialization and urbanization, protection of the environment is facing enormous challenges. Among these, water pollution has been gaining extensive attention, in particular, pollution by heavy metals (such as Cr, Cd, Pb, and Mn) from the electroplating and electronics industry. Porous[19,20] and layered[21–23] materials and ion-exchange resins[24,25] are widely used in the removal of heavy metal ions in wastewater. Yet, how to properly dispose of these materials that contain a large amount of toxic pollutants has remained a great challenge.[26–29] This is the primary motivation of the present study where we demonstrate that these waste materials might be converted into functional catalysts by simple pyrolysis, for instance, HER.

It is within this context that the present work was conceived and carried out. Herein, ion-exchange resin, used for the removal of heavy metal ions, was pyrolyzed at elevated temperatures to prepare highly active metal–carbon hybrid catalysts for HER. The immediate benefits are at least two-fold: preparation of effective catalysts from "waste" materials, and mitigation of secondary pollution by toxic heavy metals-containing ion-exchange resins. Experimentally, the synthetic process of metal–carbon hybrids was shown in Figure S1 in the Supporting Information. The ion-exchange resin (Figure S2, Supporting Information) was first soaked into a heavy metal salt solution, where the ion exchange reaction between Na^+ and M^{n+} (heavy metal ions) occurred (Step a). The pretreated resin was then transformed into porous active carbon containing a uniform distribution of metal (oxide) nanoparticles by calcination at 700 °C in a N_2 atmosphere for 2 h (Step b), which served as effective electrocatalysts for HER (Step c). For the first time, Cr–carbon electrocatalysts with efficient HER performance were synthesized from ion-exchange resin containing Cr. In addition, a variety of metal–carbon compounds, including Fe–C, Pb–C, Co–C, Ni–C, Ag–C, Mn–C, Cd–C, and Zn–C, were prepared.

2. Result and Discussion

The structure and morphology of the metal–carbon hybrids were first studied by scanning electron microscope (SEM) and transmission electron microscope (TEM) measurements. **Figure 1**a depicts a representative SEM image of the Cr–C hybrids which exhibited agglomerated blocks (500 to 1000 nm) with a rather rough surface decorated with a large number of small particulates. The corresponding X-ray diffraction (XRD) patterns (Figure 1b) show a series of diffraction peaks (#) at 33.6°, 36.2°, 54.8°, and 65.1°, corresponding to the (104), (110), (116), and (300) crystalline planes of Cr_2O_3 (JCPDS no. 38-1479), suggesting the successful incorporation of chromium into the resin which was then converted to Cr_2O_3 in the hybrids by pyrolysis (NaCl was the other product of the ion exchange reaction and manifested by diffraction peaks marked with an asterisk). In addition, graphitization of the resin by pyrolysis was confirmed by Raman spectroscopic measurements (Figure 1c) where the graphitic D and G bands can be clearly identified at

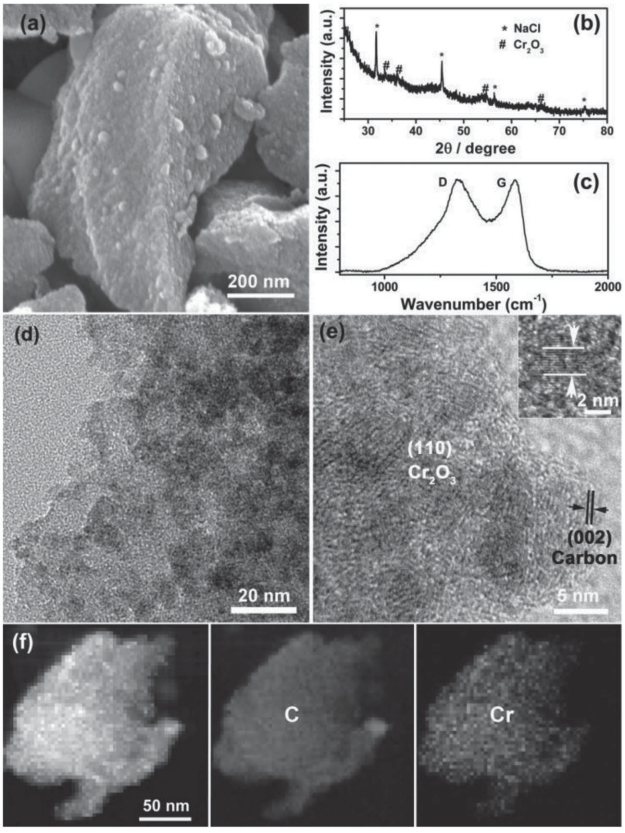

Figure 1. a) SEM image, b) XRD patterns, c) Raman spectrum, d,e) TEM images, and f) the corresponding EDX elemental mapping images of C and Cr of Cr–C hybrids. Inset to panel (e) is a high-resolution image of a Cr–C hybrid nanoparticle.

1325.7 and 1583 cm^{-1}, respectively. These results suggest the formation of a Cr–C composite.

Further structural evidence was obtained in TEM measurements. From Figure 1d,e, it can be seen that a number of crystalline nanoparticles of about 3–6 nm in diameter were homogeneously dispersed in a low-contrast framework that is most likely the carbon. The nanoparticles exhibited clearly-defined lattice fringes with a spacing of 0.24 nm that is consistent with the (110) crystalline planes of Cr_2O_3 (inset to Figure 1e). Meanwhile, the carbon layer also exhibited apparent lattice fringes and the spacing of 0.34 nm corresponded to the graphite (002) planes. Energy dispersive spectrometer (EDS)-based elemental mapping (Figure 1f) further confirmed the homogeneous distribution of Cr within C, which also confirmed that the Cr_2O_3 nanoparticles are very small. It is worth noting that nitrogen adsorption/desorption studies showed that the specific surface area of the composite was 214.5 $m^2\ g^{-1}$ (Figure S3, Supporting Information).

The elemental composition of the Cr–C hybrids was then quantified by X-ray photoelectron spectroscopic (XPS) measurements. From the survey spectrum in **Figure 2**a, the elements of C, O, and Cr can be clearly identified (NaCl was removed by water washing). A high-resolution scan of the C1s electrons (inset to Figure 2a) showed two major peaks at 284.5 and 288.5 eV, corresponding to Csp^2 and C–O, respectively. For the Cr2p electrons, deconvolution of the spectrum (Figure 2b) yielded a doublet at 576.7 and 586.4 eV,

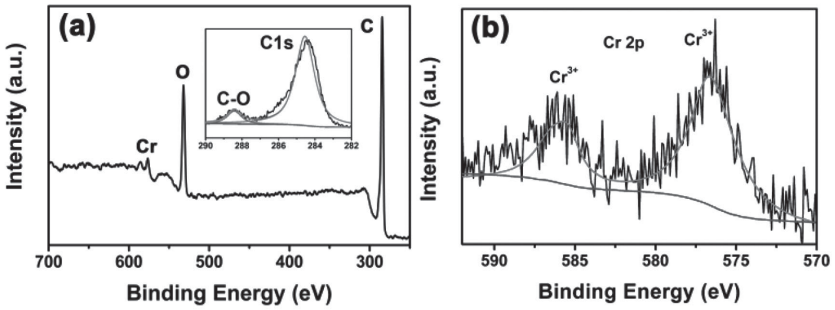

Figure 2. a) XPS survey spectrum and b) high-resolution scan of Cr 2p electrons of the Cr–C hybrids. Inset to panel (a) is the high-resolution scan of the C 1s electrons. Black curves are experimental data and grey curves are deconvolution fits.

attributable to Cr_2O_3 of Cr^{3+}, which is consistent with XRD results (Figure 1b). In fact, Cr_2O_3 was not reduced by carbon at 700 °C at the inert atmosphere, even at the H_2 atmosphere with same calcination process (Figure S4, Supporting Information), which confirmed that the Cr^{3+} is a stable low valence state. It is noteworthy that, compared with those of pure standard Cr_2O_3 (575.6 eV), the peak position of Cr–C hybrids shift positively about 1.1 eV, which implied that electron transfer likely occurred from the Cr_2O_3 nanoparticles into the carbon. Based on the integrated peak areas of the C1s and Cr 2p electrons, the concentration of Cr in the Cr–C hybrids was estimated to be 1.6 at%.

The HER activity of the Cr–C hybrids was then examined by voltammetric measurements in 0.5 M H_2SO_4. As shown in **Figure 3**a, apparent nonzero cathodic currents started to emerge when the electrode potential was swept negatively, with an onset potential of –49 mV (vs RHE, defined as the potential at which a current density of 1 mA cm^{-2} was achieved), whereas only minimal activity was observed with bare carbon from untreated resin at the same catalyst loading. Yet, one may notice that the activity of Cr–C remains subpar as compared to that of commercial 20 wt% Pt/C catalysts (≈0 mV). Generally, the HER current is expected to be proportional to the catalytically active surface area. As shown in Figure S5 in the Supporting Information, the Cr–C compound modified electrode exhibited a low double-layer capacitance of only 0.4 mF cm^{-2}, implying a low surface area and hence the enhanced HER activity of the Cr–C compound is unlikely due to the electrochemical area. In addition, only an overpotential of –123 mV was needed to reach a current density of 10 mA cm^{-2}, respectively, at the Cr–C modified electrode. This HER performance is better than or similar with the leading results about metal–carbon electrocatalysts (Table S1, Supporting Information), such as MoS_2/graphene hybrids (–150 mV),[30] CoS_2/reduced graphene oxides-carbon nanotubes (–142 mV),[8] C_3N_4@N doped graphene nanosheets (–240 mV),[31] and cobalt embedded nitrogen-rich carbon nanotubes (–260 mV).[32]

Further insights into the HER kinetics were obtained from analysis of the Tafel slope, where typically a smaller

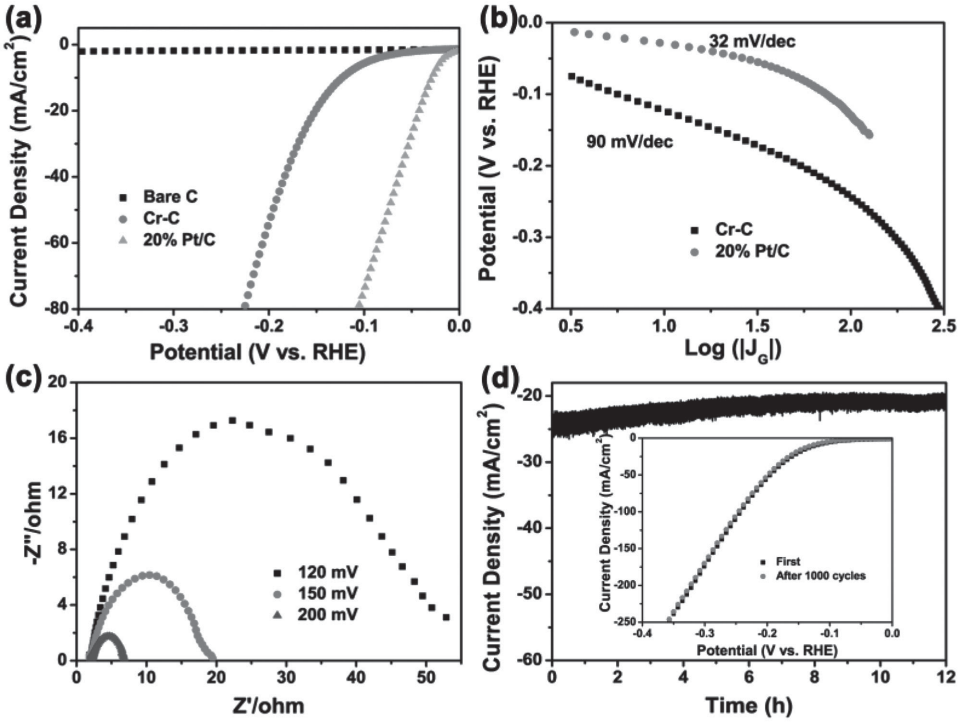

Figure 3. a) Polarization curves for HER in 0.5 M H_2SO_4 on a glassy carbon (GC) electrode modified with bare carbon from pure resin, Cr–C hybrids, and 20 wt% Pt/C, respectively. Potential sweep rate 5 mV s^{-1}. b) The corresponding Tafel plots (overpotential versus log current density) derived from (a). c) Nyquist plots of the Cr–C modified electrode at various overpotentials for HER in 0.5 M H_2SO_4. d) Current–time plots of the Cr–C modified electrode at the applied potential of –0.18 V (vs RHE). Inset to panel (d) are HER polarization curves before and after 1000 cycles in the stability test.

slope suggests a better catalytic activity. Generally, there are three reaction steps for HER in acidic electrolytes, including a primary discharge step (Volmer reaction, with a Tafel slope of 120 mV dec^{-1}) followed by an electrochemical desorption step (Heyrovsky reaction, with a Tafel slope of 40 mV dec^{-1}) or a recombination step of hydrogen adsorption on catalyst surfaces (Tafel reaction, with a Tafel slope of 30 mV dec^{-1}).[33–36] Therefore, the linear portions of the Tafel plots are fitted to the Tafel equation ($\eta = b \log j + a$, where j is the current density and b is the Tafel slope), yielding Taf l slopes of 90 and 32 mV dec^{-1} for the Cr–C hybrids and 20 wt% Pt/C, respectively (Figure 3b). The results suggest that the rate-determining step in HER was likely the Volmer–Heyrovsky reaction at the Cr–C electrode. Additionally, the HER kinetics at the electrode/electrolyte interface was probed by electrochemical impedance measurements. Figure 3c shows the representative Nyquist plots of the Cr–C catalyst modified glassy carbon (GC) electrode at various overpotentials. It can be seen that with increasing overpotential, the diameter of the semicircle in the low frequency region decreased accordingly, suggesting a diminishment of the charge transfer resistance (Rct), 52.1 Ω at –120 mV, 19.5 Ω at –150 mV, and 4.9 Ω at –200 mV.

In addition to good catalytic activity, durability is another important parameter to evaluate the HER performance. As shown in the inset to Figure 3d, the catalytic performance of Cr–C remained virtually unchanged after 1000 potential cycles. Moreover, after 12 h's continuous operation at the applied potential of –0.18 V (vs RHE), the current density of Cr–C only decreased slightly, once again confirming the remarkable HER stability in 0.5 M H_2SO_4 solution (Figure 3d)—this slight decrease of catalytic current was actually due to the formation of hydrogen bubbles on the electrode surface. The gas was confirmed to be hydrogen by gas chromatography measurements, and linear regressions of the amount of hydrogen produced at different reaction time yield the corresponding hydrogen production rate of 38.46 mmol g^{-1} h^{-1} (Figure S6, Supporting Information). O_2 produced from counter electrode (carbon cloth) was also quantified by gas chromatography with the production rate of 18.12 mmol g^{-1} h^{-1}. H_2 and O_2 evolution proceeded continuously in a molar ratio of H_2/O_2 of 2.1, effectively close to the theoretical value of 2 for overall water splitting.

In addition, the effect of calcination temperatures on the HER performance of Cr–C hybrid materials were studied. The similar agglomerated blocks with a rather rough surface were observed for all Cr–C hybrids obtained at 600, 800, and 900 °C, as shown in Figure S7a–c in the Supporting Information. The XRD results showed the Cr_2O_3 was still the main crystal phase in Cr–C hybrid, even at high calcination temperature of 900 °C (Figure S7d, Supporting Information). The Cr–C hybrid obtained at 700 °C possesses the best HER performance (–196 mV, 20 mA cm^{-2}), which was better than those of samples obtained at 600 °C (–252 mV), 800 °C (–252 mV), and 900 °C (–304 mV), as shown in Figure S8 in the Supporting Information.

The impact of the metal elements embedded within the carbon on the HER activity was then examined by soaking the resin in solution of other metal salts and preparing the M–C hybrids in a similar fashion. Note that the metal salts were chosen to mimic those commonly found in electroplating wastewater, such as Fe^{3+}, Pb^{2+}, Cr^{3+}, Co^{2+}, Ni^{2+}, Ag^{+}, Mn^{2+}, Cd^{2+}, and Zn^{2+}. Photographs of the resin after ion exchange reactions with these metal salts are shown in Figure S9 in the Supporting Information, and the elemental valence and concentrations were determined by XPS measurements (Figure S10, Supporting Information), which were summarized in Table S2 in the Supporting Information.

The electrocatalytic activities of the metal–carbon hybrids were then examined and compared. From **Figure 4**a, apparent nonzero cathodic currents can be seen at the electrode modified by all metal–carbon composites, except for carbon from pure resin. However, HER activities are remarkably different among the different metals–carbon compounds. As shown in Figure 4b, the overpotential of Fe–C at a current density of 10 mA cm^{-2} is the lowest (–60 mV vs RHE) among the series, which increased in the order of Fe–C (–60 mV), Pb–C (–119 mV), Cr–C (–123 mV), Co–C (–220 mV), Ni–C (–230 mV), Ag–C (–307 mV), Mn–C (–371 mV), Cd–C (–436 mV), and Zn–C (–471 mV). However, this is a qualitative comparison among the different metal–carbon hybrids due to the different metal contents. The highest HER activity of Fe–C hybrid is consistent with the reported Fe@carbon nanotube electrocatalysts.[16,32] However, Fe ions are not serious pollutants. In consideration of taking advantage of the abundant waste resources, the toxic heavy metals-containing ion-exchange resins (Cr) were used to produce effective HER electrocatalysts. From the Tafel plots (Figure 4c,d), it can be seen that Fe–C exhibits the lowest Tafel slope of 83 mV dec^{-1} among all the samples, with similar results observed with Co–C (89 mV dec^{-1}), Cr–C (90 mV dec^{-1}), Pb–C (88 mV dec^{-1}), and Ni–C (93 mV dec^{-1}).

Based on the above results, in conjunction with recent studies of metal@carbon-based electrocatalysts (Co, Ni, Fe, etc), the following possible synergistic catalytic effects are proposed to account for the enhanced HER catalytic activity of Cr–C. First, as for the reported electrocatalysts of Fe@C, Co@C, CoNi@C and Ag@C for HER, the metal nanoparticles not only decreased local work function on the carbon surface but also changed the electronic density of states around the carbon, resulting in the generation of additional catalytic active sites from carbon atoms.[16,18,32,37] Herein, Cr–C electrocatalyst with the high HER performance synthesized from ion-exchange resin containing Cr was reported for the first time. However, the above speculation about catalytic active sites of metal@carbon still applies to Cr–C. XPS result also confirmed that electron transfer likely occurred from the Cr_2O_3 nanoparticles into the carbon (Figure 2b). Second,some results about the enhanced HER performance by the promotion of Cr compound have been reported. For example, Zhuang and co-workers have theorized that decorating the Ni surface with Cr-oxide alters the electronic density of states of the Ni d-band in such a way to decrease the Ni—O bonding while retaining the Ni—H bond affinity.[38] Experimentally, Ramaswamy and co-workers have also reported that Cr_2O_3 can stabilize and enhance the HER activity of $Ni(O_x)/Cr_2O_3$.[39,40] Thus, the electrochemical results herein confirm that Cr^{3+} with rich electronic state in

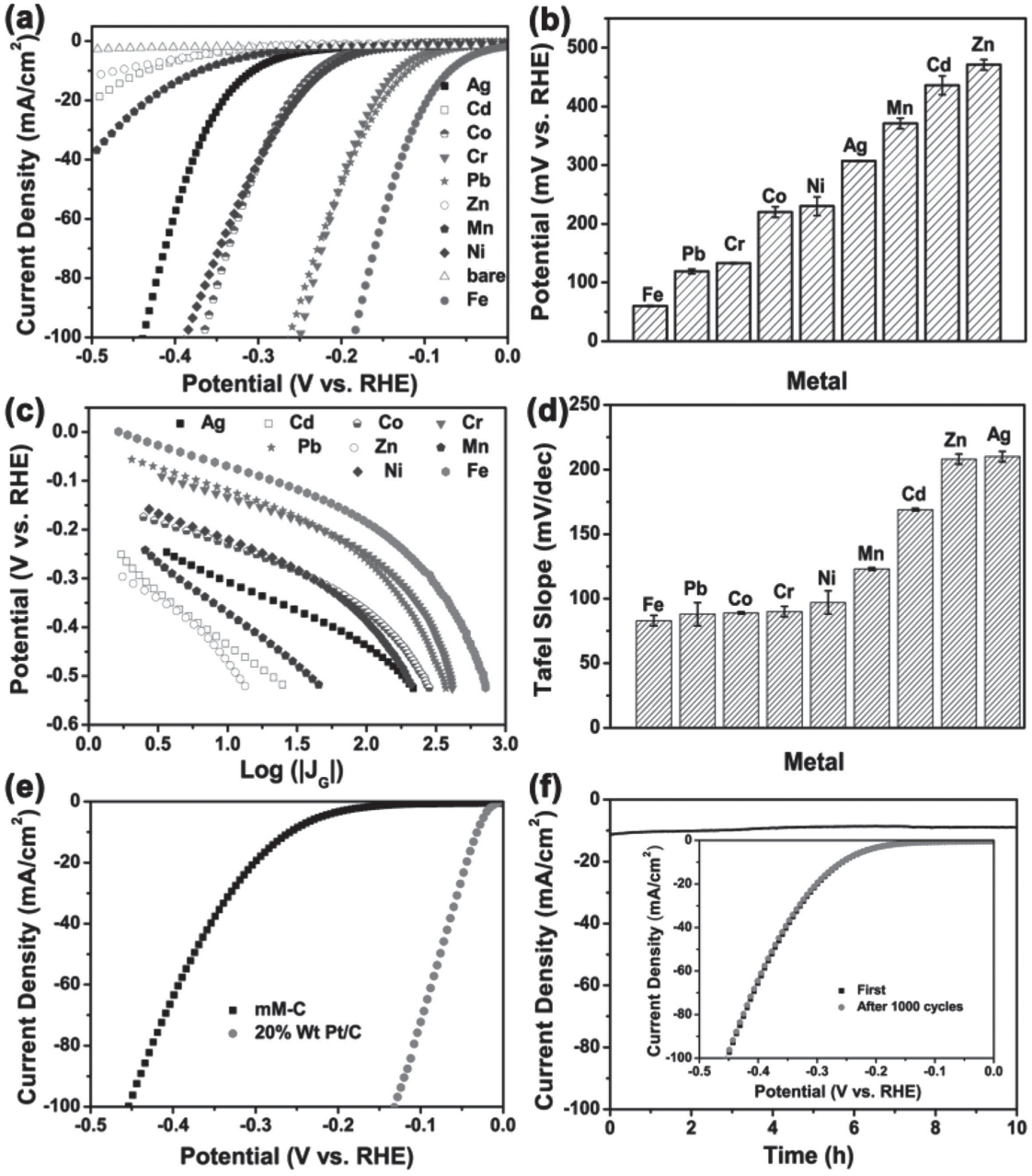

Figure 4. a) Polarization curves for HER in 0.5 M H_2SO_4 at GC electrode modified by metal–carbon compounds, including Fe–C, Pb–C, Cr–C, Co–C, Ni–C, Ag–C, Mn–C, Cd–C, and Zn–C, respectively. Potential sweep rate 5 mV s^{-1}. b) Comparison of the overpotentials of different samples at a current density of 10 mA cm^{-2}. c) Corresponding Tafel plots (overpotential versus log current density) derived from (a). d) Comparison of the Tafel slope values of different samples. e) Polarization curves for HER in 0.5 M H_2SO_4 at GC electrode modified by multimetals carbon compounds (mM–C). f) Current–time plots of the mM–C modified carbon cloth at the applied potential of –0.18 V (vs RHE). Inset to panel (f) is HER polarization curves for mM–C before and after 1000 cycles in the stability test.

the Cr–C hybrids can also modulate the electronic state density of carbon and obtain the enhanced HER activity. Third, Cr element locates in the same group with Mo and W, which possess the similar electronic structures. As is known, the catalytic activities have important relationship with the electron configuration structures of metals. The Mo (or W) based electrocatalysts with high HER activity, including MoC,[41] MoS_2,[30] and MoN,[42] implied that the similar electronic structure of Cr play the important role in enhancing the HER performance. So, we speculate that Cr compounds are also potential electrocatalytic materials for HER. Fourth, porous resin-carbon afforded highly dispersed Cr compound via ion exchange reaction and enabled rapid electron transport from the Cr_2O_3 nanoparticles to the electrodes via electronic coupling. However, the mechanistic origin of the metal–carbon compounds with the different metals is not clear. Even for mature HER electrocatalysts reported by many times, such as Co@C, CoNi@C, the catalytic mechanism was only verified

by theoretical calculations. Further in-depth studies for Cr–C hybrids are desirable.

In order to confirm the practicability of the method reported above, actual electroplating wastewater (Table S3 and Figure S10, Supporting Information) was used to undergo ion-exchange reactions with resin, and then transformed into the multimetals carbon compounds (mM–C) by the same calcination process. Electrochemical measurements showed that the obtained mM–C possesses a low overpotential of –259 mV at a current density of 10 mA cm^{-2} (Figure 4e). In addition to good catalytic activity, the mM–C modified carbon cloth also exhibits extraordinary stability for HER. Figure 4f shows that even after 1000 cycles of potential scans, the *j–V* curve of mM–C remained almost unchanged. The current–time plots at the applied potential of –0.18 V (vs RHE) also showed a stable current density of 11.2 mA cm^{-2} for 10 h, indicating long-term viability under operating conditions. The hydrogen production rate was measured to be 23.7 mmol g^{-1} h^{-1} (Figure S11, Supporting Information).

3. Conclusion

In this study, effective HER electrocatalysts based on metal–carbon composites were prepared by controlled pyrolysis of resin used to remove heavy metals at elevated temperatures (700 °C). By ion exchange reaction, Cr_2O_3 nanoparticles of 3–6 nm in diameter were found to be homogeneously dispersed in the resulting porous carbon framework, as confirmed by TEM, SEM, and nitrogen adsorption–desorption measurements. XPS results confirmed that electron transfer likely occurred from the Cr_2O_3 nanoparticles into the carbon, which is consistent with reported metal@carbon electrocatalysts. Electrochemical measurements showed that the Cr–C hybrids displayed a high HER activity with a small onset potential of only –49 mV (vs RHE), a Tafel slope of 90 mV dec^{-1}, a large catalytic current density of 10 mA cm^{-2} at –123 mV, and the prominent electrochemical durability. Further studies were extended to a wide variety of other metal ions. The obtained correlation between metal elements and HER activities may be exploited as a rational guideline in the design and engineering of functional nanocomposites for HER catalysis, in particular, based on inexpensive, abundant biowastes.

4. Experimental Section

Materials: 732 ion-exchange resin, iron nitrate ($Fe(NO_3)_3{\cdot}9H_2O$), chromium chloride hexahydrate ($CrCl_3{\cdot}6H_2O$), silver nitrate ($AgNO_3$), lead nitrate ($Pb(NO_3)_2$), cobalt sulfate ($CoSO_4{\cdot}7H_2O$), nickel chloride ($NiCl_2{\cdot}6H_2O$), silver nitrate ($AgNO_3$), manganese sulphate ($MnSO_4{\cdot}4H_2O$), cadmium nitrate ($Cd(NO_3)_2$), zinc chloride ($ZnCl_2$), and 20 wt% Pt/C were obtained from Sinopharm Chemical Reagents Beijing Co. All reagents were of analytical grade and used without further purification. Water was supplied with a Barnstead Nanopure Water System (18.3 Mcm).

Synthesis of Metal–Carbon Hybrids: In a typical experiment, 5 g of ion-exchange resin was soaked in 20 mL of a 0.5 M solution of a selected metal salt for 24 h. The resin was then filtered out and dried before being put onto a ceramic boat and calcined at 700 °C in a N_2 atmosphere for 2 h, affording metal–carbon hybrids which were denoted as M–C. The selected metal ions include Fe, Pb, Cr, Co, Ni, Ag, Mn, Cd, and Zn. In addition, electroplating wastewater containing Cr, Cu, Ni, Zn, Fe, Al, and Pb ions (composition in Table S3, Supporting Information) was used to synthesize multimetal carbon hybrids (mM–C) in a similar fashion.

Characterization: Field-emission scanning electron microscopic (NOVA NanoSEM 430, FEI) measurements were carried out to characterize the morphologies of the obtained samples. Transmission electron microscopic measurements were performed with a JOEL JEM 2100F microscope. Powder XRD patterns of the samples were recorded on a Bruker D8 Advance powder X-ray diffractometer with Cu$K\alpha$ ($\lambda = 0.15406$ nm) radiation. XPS spectra were acquired with a PHI X-tool instrument (Ulvac-Phi). Raman spectra were recorded on a RENISHAW in Via instrument with an Ar laser source of 488 nm in a macroscopic configuration. Brunauer-Emmett-Teller (BET) surface areas were quantified with a Micromeritics ASAP 2010 instrument with nitrogen adsorption at 77 K and the Barrett–Joyner–Halenda method.

Electrochemistry: Electrochemical measurements were performed with an electrochemical workstation (CHI 760C, CH Instruments Inc.) in a 0.5 m H_2SO_4 aqueous solution. A Hg/Hg_2Cl_2 electrode (saturated KCl) and carbon cloth (1×1 cm^2) were used as the reference and counter electrode, respectively. 5 mg of the catalyst powders were dispersed in 1 mL of 1:1 (v/v) water/ethanol mixed solvents, along with 80 µL of a Nafion solution, under sonication for 30 min. Then, 5 µL of the above solution was dropcast onto the surface of a GC disk electrode. The as-prepared catalyst film was dried at room temperature. Polarization curves were obtained by sweeping the potential from 0 to –0.5 V (vs RHE) at a potential sweep rate of 5 mV s^{-1}. Accelerated stability tests were performed in 0.5 m H_2SO_4 at room temperature by potential cycling between +0.3 and –0.3 V (vs RHE) at a sweep rate of 100 mV s^{-1} for 1000 cycles. Electrochemical impedance spectroscopy (EIS) spectra were acquired at an amplitude of 10 mV within the frequency range of 100 kHz to 0.01 Hz. The main arc in the EIS spectrum was fitted using a simplified Randles equivalent circuit, which consisted of a solution resistance (*R*s) in series with a parallel arrangement of a charge-transfer resistance (*R*ct) and a constant phase element, and the fitting parameters were estimated through the application of the Levenberg–Marquardt minimization procedure. Cyclic voltammetry (CV) was used to probe the electrochemical double layer capacitance at nonfaradaic potentials as a means to estimate the effective electrode surface area. Current–time responses were monitored by chronoamperometric measurements. Hydrogen production at the metal–carbon hybrids-modified carbon cloth electrode was carried out at –0.18 V (vs RHE). The gas production rate was quantified by gas chromatographic measurements (GC-2060F, LuNan Analytical Instruments, LTD, China).

In all measurements, the Hg/Hg_2Cl_2 reference electrode (in saturated KCl) was calibrated with respect to a RHE. The calibration was performed in a high-purity H_2 (99.999%) saturated electrolyte with a Pt wire as the working electrode and counter electrode. CVs were collected at a scan rate of 1 mV s^{-1}, and the average of the two potentials at which the current crossed

zero was taken as the thermodynamic potential for the hydrogen electrode reactions.

Supporting Information

Supporting Information is available from the Wiley Online Library or from the author.

Acknowledgements

This work was supported by the National Recruitment Program of Global Experts, Zhujiang New Stars of Science & Technology (2014J2200061), the Project of Public Interest Research and Capacity Building of Guangdong Province (2014A010106005), the Fundamental Research Funds for the Central Universities (D2153880), and the National Natural Science Foundation of China (51502096).

[1] M. G. Walter, E. L. Warren, J. R. McKone, S. W. Boettcher, Q. Mi, E. A. Santori, N. S. Lewis, *Chem. Rev.* **2010**, *110*, 6446.
[2] J. Luo, J.-H. Im, M. T. Mayer, M. Schreier, M. K. Nazeeruddin, N.-G. Park, S. D. Tilley, H. J. Fan, M. Grätzel, *Science* **2014**, *345*, 1593.
[3] R. Sathre, C. D. Scown, W. R. Morrow, J. C. Stevens, I. D. Sharp, J. W. Ager, K. Walczak, F. A. Houle, J. B. Greenblatt, *Energy Environ. Sci.* **2014**, *7*, 3264.
[4] R. Subbaraman, D. Tripkovic, D. Strmcnik, K.-C. Chang, M. Uchimura, A. P. Paulikas, V. Stamenkovic, N. M. Markovic, *Science* **2011**, *334*, 1256.
[5] D. Hou, W. Zhou, X. Liu, K. Zhou, J. Xie, G. Li, S. Chen, *Electrochim. Acta* **2015**, *166*, 26.
[6] S. Bai, C. Wang, M. Deng, M. Gong, Y. Bai, J. Jiang, Y. Xiong, *Angew. Chem., Int. Ed.* **2014**, *53*, 12120.
[7] J. R. McKone, N. S. Lewis, H. B. Gray, *Chem. Mater.* **2014**, *26*, 407.
[8] S. Peng, L. Li, X. Han, W. Sun, M. Srinivasan, S. G. Mhaisalkar, F. Cheng, Q. Yan, J. Chen, S. Ramakrishna, *Angew. Chem., Int. Ed.* **2014**, *53*, 12594.
[9] Y. Yang, H. Fei, G. Ruan, C. Xiang, J. M. Tour, *Adv. Mater.* **2014**, *26*, 8163.
[10] J. Yang, H. S. Shin, *J. Mater. Chem. A* **2014**, *2*, 5979.
[11] H. B. Wu, B. Y. Xia, L. Yu, X.-Y. Yu, X. W. Lou, *Nat. Commun.* **2015**, 6, 6512.
[12] Y. Zhou, Y. Leng, W. Zhou, J. Huang, M. Zhao, J. Zhan, C. Feng, Z. Tang, S. Chen, H. Liu, *Nano Energy* **2015**, *16*, 357.
[13] W. Zhou, Y. Zhou, L. Yang, J. Huang, Y. Ke, K. Zhou, L. Li, S. Chen, *J. Mater. Chem. A* **2015**, *3*, 1915.
[14] D. Deng, L. Yu, X. Chen, G. Wang, L. Jin, X. Pan, J. Deng, G. Sun, X. Bao, *Angew. Chem., Int. Ed.* **2013**, *52*, 371.
[15] J. Deng, P. Ren, D. Deng, L. Yu, F. Yang, X. Bao, *Energy Environ. Sci.* **2014**, *7*, 1919.
[16] J. Deng, P. Ren, D. Deng, X. Bao, *Angew. Chem., Int. Ed.* **2015**, *54*, 2100.
[17] J. Deng, L. Yu, D. Deng, X. Chen, F. Yang, X. Bao, *J. Mater. Chem. A* **2013**, *1*, 14868.
[18] M. Tavakkoli, T. Kallio, O. Reynaud, A. G. Nasibulin, C. Johans, J. Sainio, H. Jiang, E. I. Kauppinen, K. Laasonen, *Angew. Chem.* **2015**, *127*, 4618.
[19] J. Zhao, Z. Li, J. Wang, Q. Li, X. Wang, *J. Mater. Chem. A* **2015**, *3*, 15124.
[20] Y. Wang, G. Ye, H. Chen, X. Hu, Z. Niu, S. Ma, *J. Mater. Chem. A* **2015**, *3*, 15292.
[21] X. Lv, Z. Chen, Y. Wang, F. Huang, Z. Lin, *ACS Appl. Mater. Interfaces* **2013**, *5*, 11271.
[22] S.-Y. Wang, Y.-K. Tang, K. Li, Y.-Y. Mo, H.-F. Li, Z.-Q. Gu, *Bioresour. Technol.* **2014**, *174*, 67.
[23] L.-N. Shi, X. Zhang, Z.-L. Chen, *Water Res.* **2011**, *45*, 886.
[24] F.-B. Liang, Y.-L. Song, C.-P. Huang, Y.-X. Li, B.-H. Chen, *Ind. Eng. Chem. Res.* **2013**, *52*, 1267.
[25] A. Mahmoud, A. F. A. Hoadley, *Water Res.* **2012**, *46*, 3364.
[26] Y. Zhao, Z. He, Z. Yan, *Analyst* **2013**, *138*, 559.
[27] K. Zhou, W. Zhou, X. Liu, Y. Wang, J. Wan, S. Chen, *ACS Appl. Mater. Interfaces* **2014**, *6*, 14911.
[28] R. Wang, J. Yang, K. Shi, B. Wang, L. Wang, G. Tian, B. Bateer, C. Tian, P. Shen, H. Fu, *RSC Adv.* **2013**, *3*, 4771.
[29] P. Tao, J. Hu, W. Wang, S. Wang, M. Li, H. Zhong, Y. Tang, Z. Lu, *RSC Adv.* **2014**, *4*, 13518.
[30] Y. Li, H. Wang, L. Xie, Y. Liang, G. Hong, H. Dai, *J. Am. Chem. Soc.* **2011**, *133*, 7296.
[31] Y. Zheng, Y. Jiao, Y. Zhu, L. H. Li, Y. Han, Y. Chen, A. Du, M. Jaroniec, S. Z. Qiao, *Nat. Commun.* **2014**, *5*, 3783.
[32] X. Zou, X. Huang, A. Goswami, R. Silva, B. R. Sathe, E. Mikmeková, T. Asefa, *Angew. Chem.* **2014**, *126*, 4461.
[33] J. G. N. Thomas, *Trans. Faraday Soc.* **1961**, *57*, 1603.
[34] Z. Chen, D. Cummins, B. N. Reinecke, E. Clark, M. K. Sunkara, T. F. Jaramillo, *Nano Lett.* **2011**, *11*, 4168.
[35] W. Zhou, D. Hou, Y. Sang, S. Yao, J. Zhou, G. Li, L. Li, H. Liu, S. Chen, *J. Mater. Chem. A* **2014**, *2*, 11358.
[36] J. Duan, S. Chen, M. Jaroniec, S. Z. Qiao, *ACS Nano* **2015**, *9*, 931.
[37] Z. Zhao, P. Wang, X. Xu, M. Sheves, Y. Jin, *J. Am. Chem. Soc.* **2015**, *137*, 2840.
[38] S. Lu, J. Pan, A. Huang, L. Zhuang, J. Lu, *Proc. Natl. Acad. Sci. USA* **2008**, *105*, 20611.
[39] M. K. Bates, Q. Jia, N. Ramaswamy, R. J. Allen, S. Mukerjee, *J. Phys. Chem. C* **2015**, *119*, 5467.
[40] M. Gong, W. Zhou, M. J. Kenney, R. Kapusta, S. Cowley, Y. Wu, B. Lu, M. C. Lin, D. Y. Wang, J. Yang, *Angew. Chem.* **2015**, *127*, 12157.
[41] L. Liao, S. Wang, J. Xiao, X. Bian, Y. Zhang, M. D. Scanlon, X. Hu, Y. Tang, B. Liu, H. H. Girault, *Energy Environ. Sci.* **2014**, *7*, 387.
[42] W. F. Chen, K. Sasaki, C. Ma, A. I. Frenkel, N. Marinkovic, J. T. Muckerman, Y. Zhu, R. R. Adzic, *Angew. Chem., Int. Ed.* **2012**, *51*, 6131.

Received: October 13, 2015
Revised: January 8, 2016
Published online: April 7, 2016